BELLE2-CONF-PH-2021-04
May 10, 2021

Measurement of the time-integrated mixing probability χ_d with a semileptonic double-tagging strategy and 34.6 fb^{-1} of Belle II collision data

(The Belle II Collaboration)

Abstract

We present the first measurement of the time-integrated mixing probability χ_d using Belle II collision data corresponding to the integrated luminosity of 34.6 fb^{-1}. We reconstruct pairs of B mesons both decaying in semileptonic final states. Using a novel extraction methodology, we measure $\chi_d = 0.187 \pm 0.010$ (stat.) $\pm\, 0.019$ (syst.), which is compatible with existing indirect and direct determinations.

1. INTRODUCTION

The properties guiding the time evolution of the neutral $B^0 - \overline{B}^0$ meson system has been studied by a great number of experiments. $B^0 - \overline{B}^0$ mixing was first reported by the ARGUS experiment in Ref. [1] and the observed level of mixing provided first indications for the mass scale of the top quark. When produced in a $\Upsilon(4S)$ decay, the two B^0 mesons evolve in a coherent P-wave state. For this reason the neutral B mesons' flavour in the coherent quantum state always strictly maintain opposite flavors. As such, the B mesons' flavour can only be determined relative to each other as soon as one of the mesons decays. The mixing properties of the $B^0 - \overline{B}^0$ system can be described by four parameters (x_d, y_d, q, and p) and its time evolution is described by the Schrödinger equation, which depends on the relative time difference between the two neutral B meson decays. The heavy (H) and light (L) mass eigenstates of the system are related to the B^0 and $\overline{B}^0$ flavor eigenstates by the equation:

$$|B_{L/H}\rangle = p|B^0_d\rangle \pm q|\overline{B}^0_d\rangle \,. \tag{1}$$

In the absence of CP violation in mixing unitarity is conserved, $|q/p| = 1$, and we can express x_p and y_p as a function of the mass difference, $\Delta m_d = m_H - m_L$, and the lifetime difference, $\Delta\Gamma_d = \Gamma_L - \Gamma_H$ of the two mass eigenstates:

$$x_d = \Delta m_d/\Gamma_d \,, \qquad y_d = \Delta\Gamma_d/\Gamma_d \,, \tag{2}$$

with $\Gamma_d = (\Gamma_L + \Gamma_H)/2$ the average decay width. Experimentally, both parameters can be constrained by measuring the time-integrated mixing probability,

$$\chi_d = \frac{\Gamma(B^0 \to \overline{B}^0)}{\Gamma(B^0 \to B^0) + \Gamma(B^0 \to \overline{B}^0)} = \frac{x_d^2 + y_d^2}{2(x_d^2 + 1)} \,, \tag{3}$$

and the value of y_d can be determined in combination with direct measurements of Δm_d and the B meson lifetime. The current most precise value of χ_d is obtained by combining the information from time-independent and time-dependent measurements: $\chi_d^{\mathrm{WA}} = 0.186 \pm 0.001$ [2]. The world average obtained using only time-independent measurements has a much larger uncertainty and results in $\chi_d^{\mathrm{WA}\,t-\mathrm{in.}} = 0.182 \pm 0.015$.

In this conference note, we provide the first direct determination of χ_d using a time-independent approach and semileptonic $B \to X\, e^+\, \nu_e$ decays, recorded by the Belle II data taking campaigns in 2019 and 2020. In total, we analyze an integrated luminosity of 34.6 fb^{-1} of recorded collision data, corresponding to $(37.7 \pm 0.6) \times 10^6$ of B meson pairs. We identify events in which both B mesons decayed via a semileptonic $B \to X\, e^+\, \nu_e$ transition. The value of χ_d is obtained by determining the number of $e^\pm e^\pm$ same-sign (N_{SS}) and $e^\pm e^\mp$ opposite-sign (N_{OS}) signal candidates, as the lepton charge of the semileptonic transition encodes directly the flavor of the B meson. Contributions from charged B mesons are subtracted using a correction factor r_B and the number of opposite- and same-sign events are corrected for selection and acceptance effects to determine the time-integrated mixing probability

$$\chi_d = \frac{N_{\mathrm{SS}}}{N_{\mathrm{SS}} + N_{\mathrm{OS}} \cdot (\epsilon_{\mathrm{OS}}/\epsilon_{\mathrm{SS}})^{-1}} \cdot (1 + r_B) \,. \tag{4}$$

Here, $\epsilon_{\rm OS}$ and $\epsilon_{\rm SS}$ denote the efficiency for opposite-sign and same-sign signal, respectively, derived from studies on simulated samples and corrected using data-driven methods to account for differences in particle identification and reconstruction efficiencies, with $(\epsilon_{\rm OS}/\epsilon_{\rm SS}) = 0.92 \pm 0.01$ (stat.). Further, $r_B = f_{+0} \cdot \tau_{+0}^2 = 1.2 \pm 0.1$ with $\tau_{+0} = 1.078 \pm 0.004$ denoting the charged and neutral B meson lifetime ratio and $f_{+0} = \mathcal{B}(\Upsilon(4S) \to B^+ B^-)/\mathcal{B}(\Upsilon(4S) \to B^0 \overline{B}^0) = 1.058 \pm 0.024$ [2].

2. THE BELLE II DETECTOR AND DATA SAMPLE

The Belle II detector [3, 4] operates at the SuperKEKB asymmetric-energy electron-positron collider [5], located at the KEK laboratory in Tsukuba, Japan. The detector consists of several nested detector subsystems arranged around the beam pipe in a cylindrical geometry. The innermost subsystem is the vertex detector, which includes two layers of silicon pixel and four outer layers of silicon strip detectors. Currently, the second pixel layer is installed in only a small part of the solid angle, while the remaining vertex detector layers are fully installed. Most of the tracking volume consists of a small-cell drift chamber filled with a helium and ethane mixture gas. Outside the drift chamber, a Cherenkov-light imaging and time-of-propagation detector provides charged-particle identification in the barrel region. In the forward endcap, this function is provided by a proximity-focusing, ring-imaging Cherenkov detector with an aerogel radiator. Further out is an electromagnetic calorimeter, consisting of a barrel and two endcap sections made of CsI(Tl) crystals. A uniform 1.5 T magnetic field is provided by a superconducting solenoid situated outside the calorimeter. Multiple layers of scintillators and resistive plate chambers, located between the magnetic flux-return iron plates, constitute the K_L^0 and muon identification system.

The collision data used in this analysis were collected at a center-of-mass (CM) energy of 10.58 GeV, corresponding to the mass of the Υ(4S) resonance. The energies of the electron and positron beams are 7 GeV and 4 GeV, respectively, resulting in a boost of $\beta\gamma = 0.28$ of the CM frame relative to the laboratory frame. In addition, 3.2 fb^{-1} of off-resonance collision data, collected at 60 MeV below the Υ(4S) resonance, is used to model background from e^+e^- continuum processes.

Simulated Monte Carlo (MC) samples of $B \to X\, e^+\, \nu_e$ signal and background processes are used to obtain the reconstruction efficiencies and study the key kinematic distributions. These events are generated with EvtGen [6] and the used branching fractions are summarized in Table I. Inclusive semileptonic $B \to X\, e^+\, \nu_e$ decays are dominated by $B \to D\, e^+\, \nu_e$ and $B \to D^*\, e^+\, \nu_e$ transitions. We model the $B \to D\, e^+\, \nu_e$ decays using the BGL parametrization [7] with form factor central values and uncertainties taken from the fit in Ref. [8]. For $B \to D^*\, \ell^+\, \nu_\ell$ we use the BGL implementation proposed in Refs. [9, 10] with form factor central values and uncertainties from the fit to the measurement of Ref. [11]. Both backgrounds are normalized to the average branching fraction of Ref. [12] assuming isospin symmetry. Semileptonic $B \to D^{**}\, \ell^+\, \nu_\ell$ decays with $D^{**} = \{D_0^*, D_1^*, D_1, D_2^*\}$ denoting the four orbitally excited charmed mesons are modeled using the heavy-quark-symmetry-based form factors proposed in Refs. [13, 14]. Non-resonant $B \to D^*\, \pi\ell\bar{\nu}_\ell$ are modeled using the framework of Ref. [15]. To account for the remaining 'gap' between the sum of all considered exclusive modes and the inclusive $B \to X_c\, e^+\, \nu_e$ branching fraction, the simulated data set is filled with $B \to D^{(*)}\, \pi\, \pi\, \ell^+\, \nu_\ell$ and $B \to D^{(*)}\, \eta\, \ell^+\, \nu_\ell$ decays using a model based on the

TABLE I. Branching fractions for $B \to X_c\, \ell^+\, \nu_\ell$ and $B \to X_u\, \ell^+\, \nu_\ell$ processes that were used to generate simulated samples are listed.

$\mathcal{B}$	B^+	B^0
$B \to X_c\, \ell^+\, \nu_\ell$		
$B \to D\, \ell^+\, \nu_\ell$	$(2.41 \pm 0.07) \times 10^{-2}$	$(2.24 \pm 0.07) \times 10^{-2}$
$B \to D^*\, \ell^+\, \nu_\ell$	$(5.50 \pm 0.11) \times 10^{-2}$	$(5.11 \pm 0.11) \times 10^{-2}$
$B \to D_0^*\, \ell^+\, \nu_\ell$	$(0.42 \pm 0.08) \times 10^{-2}$	$(0.39 \pm 0.07) \times 10^{-2}$
$B \to D_1^*\, \ell^+\, \nu_\ell$	$(0.42 \pm 0.09) \times 10^{-2}$	$(0.39 \pm 0.08) \times 10^{-2}$
$B \to D_1\, \ell^+\, \nu_\ell$	$(0.66 \pm 0.11) \times 10^{-2}$	$(0.62 \pm 0.10) \times 10^{-2}$
$B \to D_2^*\, \ell^+\, \nu_\ell$	$(0.29 \pm 0.03) \times 10^{-2}$	$(0.27 \pm 0.03) \times 10^{-2}$
$B \to D\pi\pi\, \ell^+\, \nu_\ell$	$(0.06 \pm 0.09) \times 10^{-2}$	$(0.06 \pm 0.09) \times 10^{-2}$
$B \to D^*\pi\pi\, \ell^+\, \nu_\ell$	$(0.22 \pm 0.10) \times 10^{-2}$	$(0.20 \pm 0.10) \times 10^{-2}$
$B \to D_s K\, \ell^+\, \nu_\ell$	$(0.03 \pm 0.01) \times 10^{-2}$	-
$B \to D_s^* K\, \ell^+\, \nu_\ell$	$(0.03 \pm 0.01) \times 10^{-2}$	-
$B \to D\eta\, \ell^+\, \nu_\ell$	$(0.41 \pm 0.41) \times 10^{-2}$	$(0.41 \pm 0.41) \times 10^{-2}$
$B \to D^*\eta\, \ell^+\, \nu_\ell$	$(0.41 \pm 0.41) \times 10^{-2}$	$(0.41 \pm 0.41) \times 10^{-2}$
$B \to X_u\, \ell^+\, \nu_\ell$	$(0.22 \pm 0.03) \times 10^{-2}$	$(0.21 \pm 0.03) \times 10^{-2}$
$B \to X\, \ell^+\, \nu_\ell$	$(10.99 \pm 0.28) \times 10^{-2}$	$(10.33 \pm 0.28) \times 10^{-2}$

equidistribution of all final-state particles in phase-space. Semileptonic $B \to X_u\, e^+\, \nu_e$ decays are modeled as a mixture of specific exclusive modes and non-resonant contributions.

3. ANALYSIS STRATEGY

Our general analysis strategy is as follows: we first identify samples of same-sign and opposite-sign di-electron candidates. We then apply a selection based on tracks and global event properties to enrich the samples with double-semileptonic $B^0 - \overline{B}^0$ ("signal") decays. For events passing the selection, we build a variable that can distinguish between signal and misreconstructed events, which is fitted to extract N_{SS} and N_{OS}. We describe these steps in more detail below.

3.1. Di-electron candidate selection

We build electron pairs from single electron candidates that satisfy the following criteria:

- High center-of-mass momentum: $|p_e^*| > 1$ GeV.
- Impact parameter consistent with the interaction point: the track must pass within 4 cm along the beam axis in the laboratory frame and within 2 cm transverse to the beam axis of the interaction point.

- High electron ID likelihood: ID > 0.9.

Each electron candidate energy is corrected for loss due to Bremsstrahlung radiation using a dedicated search algorithm that matches electromagnetic clusters in the calorimeter to electron candidates. We then separate the electron pair candidates according to the reconstructed charges into SS and OS categories.

3.2. Signal enrichment

Using the correspondence between the generated particles and the reconstructed tracks, we classify the pair as "Signal" if both electrons are daughters of different B mesons, and label the rest "Other". We use the off-resonance dataset to describe the continuum background distributions.

We use the following selections, in this order, to suppress the major backgrounds:

- *Photon and J/ψ veto*: we check whether either of the signal electron candidates can match with any opposite-sign track in the event under the electron mass hypothesis to give an invariant mass near zero ($m_{ee} < 0.2$ GeV) to reject electrons from photon conversions or near the J/ψ resonance (2.92 GeV $< m_{ee} < 3.14$ GeV). We discard di-electron candidates if such a match is found ($\epsilon_{\mathrm{SS}} = 0.958$, $\epsilon_{\mathrm{OS}} = 0.896$).
- *Best candidate selection*: if multiple di-electron pair candidates exist in an event, we randomly choose one as the sole candidate in the event ($\epsilon_{\mathrm{SS}} = 0.999$, $\epsilon_{\mathrm{OS}} = 0.990$).
- *Event track number selection*: we discard events for which there are less than five total tracks that pass the same impact parameter selections as the signal leptons ($\epsilon_{\mathrm{SS}} = 0.923$, $\epsilon_{\mathrm{OS}} = 0.917$).
- *Continuum suppression*: we retain events with a normalized Fox-Wolfram moment [16] value $R_2 < 0.3$ ($\epsilon_{\mathrm{SS}} = 0.889$, $\epsilon_{\mathrm{OS}} = 0.895$).
- *Electron ID coverage selection:* we discard events for which electron ID corrections are not available for both electron candidates ($\epsilon_{\mathrm{SS}} = 0.890$, $\epsilon_{\mathrm{OS}} = 0.894$).

After these selections, the remaining backgrounds come largely from mis-identified electrons, electron pairs where both electrons have the same common B-meson ancestor, $B \to (X_c \to X_s e^- \overline{\nu_e}) e^+ \nu_e$ (OS only), and continuum events.

3.3. The extraction variable

Our signal consists of two electrons from semileptonic B decays, each of which has a mean energy above that of the primary background sources. Therefore, the sum of the magnitude of the momentum in the center-of-mass frame of the two electrons:

$$p_{ee} = |p^*_{e1}| + |p^*_{e2}| \tag{5}$$

provides discrimination between signal and background. This variable has not been exploited thus far in time-integrated χ_d measurements. In Fig. 1 we show this spectrum in OS and SS for MC and data.

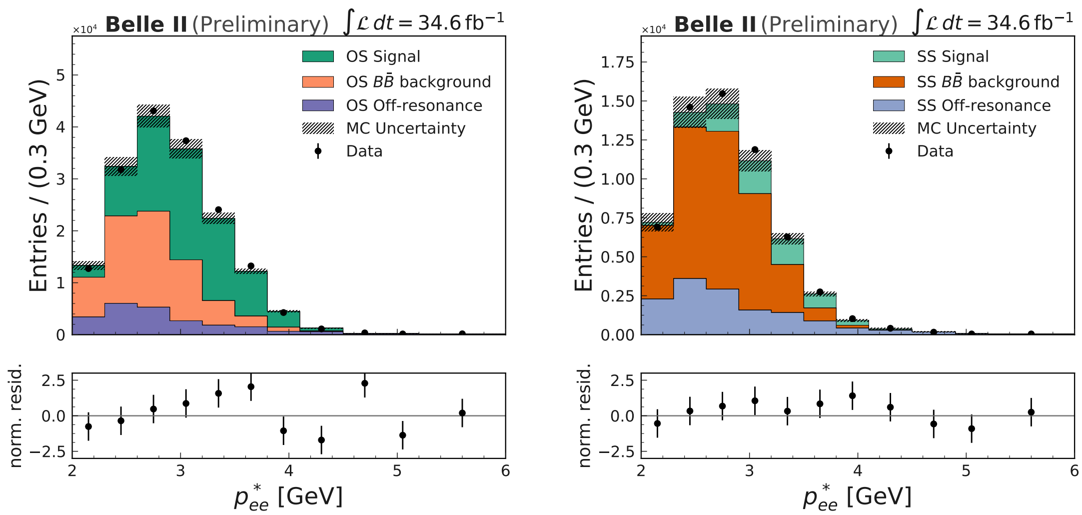

FIG. 1. The p_{ee} spectrum for opposite-sign (left) and same-sign (right) di-electron samples after all selections and before fitting. The shaded, stacked histograms show the expected spectra from the sum of "Signal" MC (green), "Other" $B\overline{B}$ MC (orange), and scaled off-resonance data (purple). The black points indicate the spectrum as measured in data. The shaded area shows the size of the systematic uncertainty from lepton identification efficiencies, signal and background shapes, and the statistical uncertainty of the off-resonance data. The lower distributions show the normalized residuals between data and MC calculated as $(N_{\mathrm{data}}-N_{\mathrm{MC}})/\sqrt{\sigma^2_{\mathrm{data}}+\sigma^2_{\mathrm{MC}}}$, where N is the number of entries, σ_{data} denotes the statistical uncertainty of the data and σ_{MC} stands for the total uncertainty of MC in each bin.

4. FITTING PROCEDURE

The number of same-sign and opposite-sign $B \to X\, e^+\, \nu_e$ candidates is determined by a simultaneous binned likelihood fit to the p_{ee} distribution of both samples and in 11 p_{ee} bins ranging from 2 - 6 GeV. For each of the 11 p_{ee} bins, the free parameters of the fit are:

a) The number of same-sign and opposite-sign $B \to X\, e^+\, \nu_e$ candidates: N_{SS}, N_{OS}

b) The number of background events in each sample from B meson decays: N_{BSS}, N_{BOS}

c) The number of background events in each sample from continuum processes: N_{CSS}, N_{COS}

and which correspond to the yields of the three event categories considered. The total likelihood function is

$$\mathcal{L} = \prod_i^{\text{bins}} \mathcal{P}\left(n_i; \nu_i\right) \times \prod_k \mathcal{G}_k\,, \tag{6}$$

with n_i denoting the number of observed data events and ν_i the total number of expected events in a given bin i. Here, $\mathcal{G}_k$ are nuisance-parameter (NP) constraints for a given template k, whose role is to incorporate systematic uncertainties and the number of expected continuum events, as determined from the off-resonance data, directly into the fit. The number of expected events in a given bin, ν_i, is estimated using MC and off-resonance data and is given by

$$\nu_i = N_{\text{SS}} \cdot f_{i,\text{SS}} + N_{\text{BSS}} \cdot f_{i,\text{BSS}} + N_{\text{CSS}} \cdot f_{i,\text{CSS}}\,, \tag{7}$$

or

$$\nu_i = N_{\text{OS}} \cdot f_{i,\text{OS}} + N_{\text{BOS}} \cdot f_{i,\text{BOS}} + N_{\text{COS}} \cdot f_{i,\text{COS}}\,, \tag{8}$$

for same-sign or opposite-sign events, respectively. Here, the f_i correspond to the fraction of events of each category being reconstructed in bin i as determined by the MC simulation or the off-resonance data. The NP constraints are constructed such that they take into account uncertainties due to the electron identification efficiency, signal and background template compositions, and the statistical uncertainty of the template in question. They are incorporated using multivariate Gaussian distributions, $\mathcal{G}_k = \mathcal{G}_k(\mathbf{0}; \boldsymbol{\theta}_k, \Sigma_k)$. Here the Σ_k denotes the systematic covariance matrix for a given template k and $\boldsymbol{\theta}_k$ is a vector of NPs. The covariance Σ_k is the sum over all possible uncertainty sources for a given template. The fractions in Eqs. 7 and 8 are allowed to change within these systematic uncertainties according to:

$$f_i = \frac{N_i^{\text{MC}}\left(1+\theta_i\right)}{\sum_j N_j^{\text{MC}}\left(1+\theta_j\right)}\,, \tag{9}$$

with N_i^{MC} denoting the number of expected events of a given category in bin i as estimated by MC, and θ_j the j^{th} element of the NP vector $\boldsymbol{\theta}_k$. The likelihood function is maximized numerically to determine all components and NP constraints. Confidence intervals for the N_{SS}, N_{OS} components are constructed using the profile likelihood ratio method.

5. RESULTS

Figure 2 shows the post-fit p_{ee} distribution for same-sign and opposite-sign candidates. The goodness-of-fit cannot be judged based on the residuals alone, but also depends on the NP pulls, which we show in Appendix A. From this fit, we measure:

$$\chi_d = 0.187 \pm 0.010\ (\text{stat.}) \pm 0.019\ (\text{syst.}) \tag{10}$$

where the first uncertainty is statistics and the second systematics [17]. The uncertainty is dominated by the statistical uncertainty of the same-sign sample, the limited size of

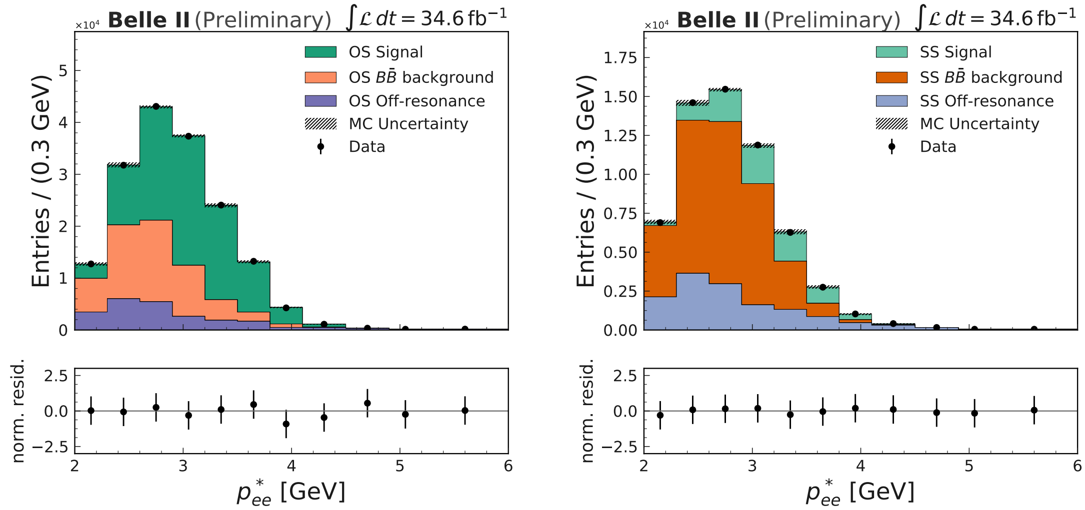

FIG. 2. The p_{ee} spectrum for opposite-sign (left) and same-sign (right) di-electron samples after fitting. The shaded, stacked histograms show the fitted spectra from the sum of "Signal" MC (green), "Other" $B\overline{B}$ MC (orange), and scaled off-resonance data (purple). The black points indicate the spectrum as measured in data. The shaded area around the MC expectation correspond to the post-fit uncertainty. The lower distributions show the normalized residuals between data and MC calculated as $(N_{\mathrm{data}} - N_{\mathrm{MC}})/\sqrt{\sigma^2_{\mathrm{data}} + \sigma^2_{\mathrm{MC}}}$, where N is the number of entries, σ_{data} denotes the statistical uncertainty of the data and σ_{MC} stands for the total uncertainty of MC in each bin..

the off-resonance data sample, and the systematic uncertainty of the electron identification corrections. The size of these systematic uncertainties is expected to decrease with larger control samples. The obtained value of χ_d is compatible with the world average from time-independent and time-dependent determinations [2] and the reported measurement already has a similar precision to the time-independent world average.

6. ACKNOWLEDGEMENTS

We thank the SuperKEKB group for the excellent operation of the accelerator; the KEK cryogenics group for the efficient operation of the solenoid; and the KEK computer group for on-site computing support. This work was supported by the following funding sources: Science Committee of the Republic of Armenia Grant No. 18T-1C180; Australian Research Council and research grant Nos. DP180102629, DP170102389, DP170102204, DP150103061, FT130100303, and FT130100018; Austrian Federal Ministry of Education, Science and Research, and Austrian Science Fund No. P 31361-N36; Natural Sciences and Engineering Research Council of Canada, Compute Canada and CANARIE; Chinese Academy of Sciences and research grant No. QYZDJ-SSW-SLH011, National Natural Science Foundation of China and research grant Nos. 11521505, 11575017, 11675166, 11761141009, 11705209, and 11975076, LiaoNing Revitalization Talents Program under contract No. XLYC1807135, Shanghai Municipal Science and Technology Committee under contract No. 19ZR1403000, Shanghai Pujiang Program under Grant No. 18PJ1401000, and the CAS Center for Excellence in Particle Physics (CCEPP); the Ministry of Education, Youth and Sports of the Czech Republic under Contract No. LTT17020 and Charles University grants SVV 260448 and GAUK 404316; European Research Council, 7th Framework PIEF-GA-2013-622527, Horizon 2020 Marie Sklodowska-Curie grant agreement No. 700525 'NIOBE,' and Horizon 2020 Marie Sklodowska-Curie RISE project JENNIFER2 grant agreement No. 822070 (European grants); L'Institut National de Physique Nucléaire et de Physique des Particules (IN2P3) du CNRS (France); BMBF, DFG, HGF, MPG, AvH Foundation, and Deutsche Forschungsgemeinschaft (DFG) under Germany's Excellence Strategy – EXC2121 "Quantum Universe"' – 390833306 (Germany); Department of Atomic Energy and Department of Science and Technology (India); Israel Science Foundation grant No. 2476/17 and United States-Israel Binational Science Foundation grant No. 2016113; Istituto Nazionale di Fisica Nucleare and the research grants BELLE2; Japan Society for the Promotion of Science, Grant-in-Aid for Scientific Research grant Nos. 16H03968, 16H03993, 16H06492, 16K05323, 17H01133, 17H05405, 18K03621, 18H03710, 18H05226, 19H00682, 26220706, and 26400255, the National Institute of Informatics, and Science Information NETwork 5 (SINET5), and the Ministry of Education, Culture, Sports, Science, and Technology (MEXT) of Japan; National Research Foundation (NRF) of Korea Grant Nos. 2016R1D1A1B01010135, 2016R1D1A1B-02012900, 2018R1A2B3003643, 2018R1A6A1A06024970, 2018R1D1A1B07047294, 2019K1-A3A7A09033840, and 2019R1I1A3A01058933, Radiation Science Research Institute, Foreign Large-size Research Facility Application Supporting project, the Global Science Experimental Data Hub Center of the Korea Institute of Science and Technology Information and KREONET/GLORIAD; Universiti Malaya RU grant, Akademi Sains Malaysia and Ministry of Education Malaysia; Frontiers of Science Program contracts FOINS-296, CB-221329, CB-236394, CB-254409, and CB-180023, and SEP-CINVESTAV research grant 237 (Mexico); the Polish Ministry of Science and Higher Education and the National Science Center; the Ministry of Science and Higher Education of the Russian Federation, Agreement 14.W03.31.0026; University of Tabuk research grants S-1440-0321, S-0256-1438, and S-0280-1439 (Saudi Arabia); Slovenian Research Agency and research grant Nos. J1-9124 and P1-0135; Agencia Estatal de Investigacion, Spain grant Nos. FPA2014-55613-P and FPA2017-84445-P, and CIDEGENT/2018/020 of Generalitat Valenciana; Ministry of Science and Technology and research grant Nos. MOST106-2112-M-002-005-MY3 and MOST107-2119-M-002-035-MY3, and the Ministry of Education (Taiwan); Thailand Center of Excellence in Physics; TUBITAK ULAKBIM (Turkey); Ministry of Education and Science of Ukraine; the US National Science Foundation and research grant Nos. PHY-1807007 and PHY-1913789, and the US Department of Energy and research grant Nos. DE-AC06-76RLO1830, DE-SC0007983, DE-SC0009824, DE-SC0009973, DE-SC0010073, DE-SC0010118, DE-SC0010504, DE-SC0011784, DE-SC0012704; and the National Foundation for Science and Technology Development (NAFOSTED) of Vietnam under contract No 103.99-2018.45.

---

[1] H. Albrecht et al., *Observation of B0-B0 mixing*, Physics Letters B **192** (1987) no. 1, 51–63.

[2] P. Zyla et al., Particle Data Group Prog. Theor. Exp. Phys. **2020 083C01** (2020) .

[3] T. Abe et al., Belle II Collaboration, *Belle II Technical Design Report*, `arXiv:1011.0352 [physics.ins-det]`.

[4] E. Kou et al., *The Belle II Physics Book*, PTEP **2019** (2019) no. 12, 123C01.

[5] K. Akai, K. Furukawa, and H. Koiso, SuperKEKB Collaboration, *SuperKEKB Collider*, Nucl. Instrum. Meth. **A907** (2018) 188–199.

[6] D. J. Lange, *The EvtGen particle decay simulation package*, Nucl. Instrum. Meth. **A462** (2001) 152–155.

[7] C. G. Boyd, B. Grinstein, and R. F. Lebed, *Constraints on form-factors for exclusive semileptonic heavy to light meson decays*, Phys. Rev. Lett. **74** (1995) 4603–4606, `arXiv:hep-ph/9412324 [hep-ph]`.

[8] R. Glattauer et al., Belle Collaboration, *Measurement of the decay $B \to D\ell\nu_\ell$ in fully reconstructed events and determination of the Cabibbo-Kobayashi-Maskawa matrix element $|V_{cb}|$*, Phys. Rev. D **93** (2016) no. 3, 032006, `arXiv:1510.03657 [hep-ex]`.

[9] B. Grinstein and A. Kobach, *Model-Independent Extraction of $|V_{cb}|$ from $\bar{B} \to D^*\ell\overline{\nu}$*, Phys. Lett. **B 771** (2017) 359–364, `arXiv:1703.08170 [hep-ph]`.

[10] D. Bigi, P. Gambino, and S. Schacht, *A fresh look at the determination of $|V_{cb}|$ from $B \to D^*\ell\nu$*, Phys. Lett. B **769** (2017) 441–445, `arXiv:1703.06124 [hep-ph]`.

[11] E. Waheed et al., Belle Collaboration, *Measurement of the CKM matrix element $|V_{cb}|$ from $B^0 \to D^{*-}\ell^+\nu_\ell$ at Belle*, Phys. Rev. D **100** (2019) no. 5, 052007, `arXiv:1809.03290 [hep-ex]`.

[12] Y. S. Amhis et al., HFLAV, *Averages of b-hadron, c-hadron, and τ-lepton properties as of 2018*, `arXiv:1909.12524 [hep-ex]`.

[13] F. U. Bernlochner and Z. Ligeti, *Semileptonic $B_{(s)}$ decays to excited charmed mesons with e, μ, τ and searching for new physics with $R(D^{**})$*, Phys. Rev. D **95** (2017) no. 1, 014022, `arXiv:1606.09300 [hep-ph]`.

[14] F. U. Bernlochner, Z. Ligeti, and D. J. Robinson, *Model independent analysis of semileptonic B decays to D^{**} for arbitrary new physics*, Phys. Rev. D **97** (2018) no. 7, 075011, `arXiv:1711.03110 [hep-ph]`.

[15] J. L. Goity and W. Roberts, *Soft pion emission in semileptonic B meson decays*, Phys. Rev. D **51** (1995) 3459–3477, `arXiv:hep-ph/9406236`.

[16] G. C. Fox and S. Wolfram, *Observables for the Analysis of Event Shapes in e^+e^- Annihilation and Other Processes*, Phys. Rev. Lett. **41** (Dec, 1978) 1581–1585. `https://link.aps.org/doi/10.1103/PhysRevLett.41.1581`.

[17] Since the conference presentation the extracted value of χ_d has shifted slightly due to improvements of the $B \to X_c\, e^+\, \nu_e$ modeling and composition.

Appendix A: Nuisance parameter pulls

We include distributions of the NP pulls from the fit shown in Fig. 2, for the signal (Fig. 3), other $B\overline{B}$ (Fig. 4), and off-resonance (Fig. 5) templates. The moderate deviation that can be seen in the pulls of the OS signal template corresponds to higher values in p_{ee} which is mostly occupied by $B \to X_u \ell^+ \nu_\ell$ decays.

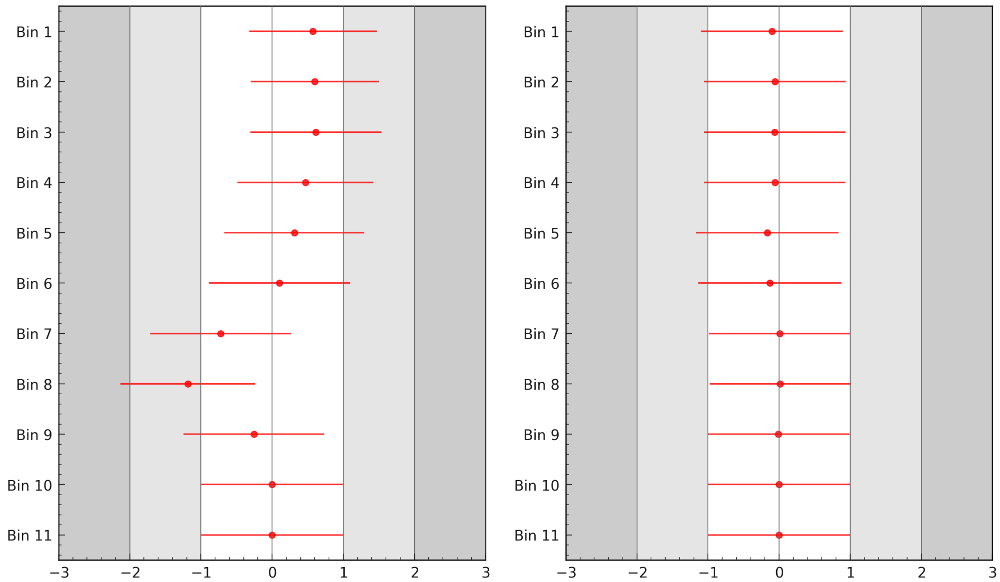

FIG. 3. Pulls on the nuisance parameters for the OS (left) and SS (right) signal templates.

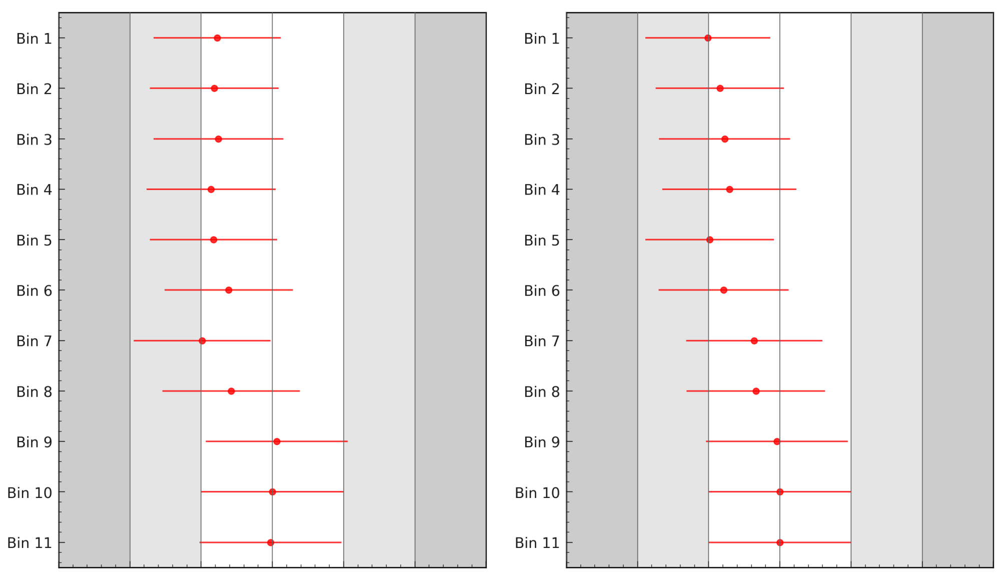

FIG. 4. Pulls on the nuisance parameters for the OS (left) and SS (right) $B\overline{B}$ background templates.

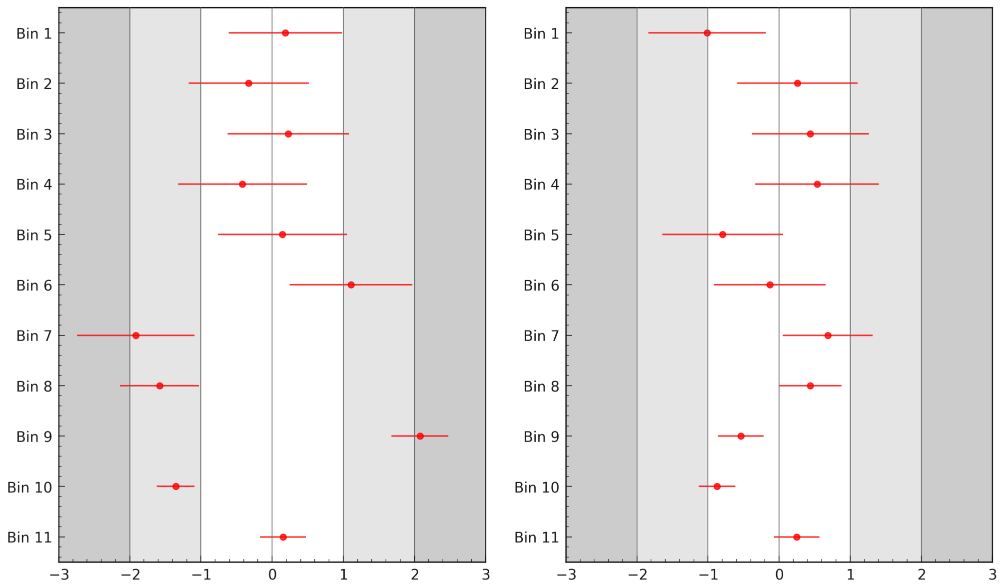

FIG. 5. Pulls on the nuisance parameters for the OS (left) and SS (right) off-resonance templates.